Optogenetic-guided cortical plasticity after nerve injury

Nan Li[a,b], John E. Downey[a], Amnon Bar-Shir[c,d], Assaf A. Gilad[a,c,d], Piotr Walczak[c,d], Heechul Kim[c,d], Suresh E. Joel[a,c], James J. Pekar[a,c], Nitish V. Thakor[b], and Galit Pelled[a,c,1]

[a]F. M. Kirby Research Center for Functional Brain Imaging, Kennedy Krieger Institute, Baltimore, MD 21205; [b]Department of Biomedical Engineering and [d]Cellular Imaging Section, Vascular Biology Program, Institute for Cell Engineering, Johns Hopkins University School of Medicine, Baltimore, MD 21205; and [c]The Russell H. Morgan Department of Radiology and Radiological Science, Johns Hopkins University School of Medicine, Baltimore, MD 21287

Edited by Jon H. Kaas, Vanderbilt University, Nashville, TN, and approved April 12, 2011 (received for review January 21, 2011)

Peripheral nerve injury causes sensory dysfunctions that are thought to be attributable to changes in neuronal activity occurring in somatosensory cortices both contralateral and ipsilateral to the injury. Recent studies suggest that distorted functional response observed in deprived primary somatosensory cortex (S1) may be the result of an increase in inhibitory interneuron activity and is mediated by the transcallosal pathway. The goal of this study was to develop a strategy to manipulate and control the transcallosal activity to facilitate appropriate plasticity by guiding the cortical reorganization in a rat model of sensory deprivation. Since transcallosal fibers originate mainly from excitatory pyramidal neurons somata situated in laminae III and V, the excitatory neurons in rat S1 were engineered to express halorhodopsin, a light-sensitive chloride pump that triggers neuronal hyperpolarization. Results from electrophysiology, optical imaging, and functional MRI measurements are concordant with that within the deprived S1, activity in response to intact forepaw electrical stimulation was significantly increased by concurrent illumination of halorhodopsin over the healthy S1. Optogenetic manipulations effectively decreased the adverse inhibition of deprived cortex and revealed the major contribution of the transcallosal projections, showing interhemispheric neuroplasticity and thus, setting a foundation to develop improved rehabilitation strategies to restore cortical functions.

recovery | amputation

Although 20 million Americans suffer from peripheral nerve injury caused by trauma, metabolic, endocrine, and autoimmune disorders, there are few strategies to promote recovery. Surgical nerve repair and training of the injured limb are the classical rehabilitation approaches. Nevertheless, the clinical outcome in adults is generally poor, with persisting sensory dysfunction and pain (1).

Recent evidence suggests that sensory dysfunctions caused by nerve injury should be attributable not only to the functional, cellular, and biochemical events occurring in peripheral nerve but also functional and anatomical changes occurring in cerebral cortical representations. It is well-documented in humans (2), non- human primates (3), cats (4), and rodents (5–7) that peripheral nerve injury can lead to expansion of neighboring cortical representation of peripheral regions within the affected (deprived) hemisphere (intrahemispheric neuroplasticity). Peripheral nerve injury and direct cortical lesions have been shown to also modify functional communication between cortical hemispheres (interhemispheric neuroplasticity) (8–19). Specifically, peripheral inputs normally evoking neuronal responses in the contralateral hemisphere cause inappropriate functional responses in the ipsilateral hemisphere. Previously, using single-unit electrophysiology recordings and juxtacellular labeling, it was shown that the inappropriate ipsilateral functional magnetic resonance imaging (fMRI) responses observed in deprived primary somatosensory cortex (S1) were accompanied by an increase in activity of inhibitory interneurons (20). Moreover, ablation of the healthy S1 completely eliminated fMRI responses in the deprived S1 when the intact limb, ipsilateral to the deprived S1, was stimulated (21). Therefore, it appears that peripheral nerve injury evokes an increase in inhibitory activity in the deprived cortical areas, which is mediated by the transcallosal pathway. Indeed, there are ongoing efforts to modify transcallosal activity in patients suffering from peripheral nerve injury. For instance, improvement in tactile discrimination of the injured hand was found after decreasing afferent inputs from the intact hand using constraint induced therapy (CIT) (22), using nerve blocking (23), and directly inhibiting neuronal networks through transcranial magnetic stimulation (TMS) (24, 25). Still, these rehabilitation approaches are neither precise nor neuronal-specific, and they cannot be repeated often. Moreover, it is not clear what neuroplasticity mechanisms are being targeted by these techniques.

The goal of this study was to develop a strategy to manipulate and control the transcallosal activity to facilitate appropriate plasticity by guiding the cortical reorganization in a rat model of sensory deprivation. We used optogenetic technologies that offer precise and transient control of the firing rates of a specific population of neurons (26, 27) to achieve modulation of the neuronal activity in the healthy, unaffected hemisphere. Recently, optogenetic approaches have been used to investigate and probe various neuronal circuits in rodents, such as the transcallosal pathway (28), epileptic activity in the hippocampus and cortex (29), and Parkinson's disease (30). Optogenetics was also applied in primates with the goal of replacing microelectrode stimulation (31).

Since transcallosal fibers originate mainly from excitatory pyramidal neurons somata situated in laminae III and V (32–35), the excitatory neurons throughout the rats S1 were engineered to express halorhodopsin (eNpHR), a light-sensitive chloride pump. Illumination of eNpHR by a specific wavelength of light triggers neuronal hyperpolarization (i.e., decrease in neuronal firing rate). To infect a large population of excitatory pyramidal neurons throughout the cortex, a lentivirus encoding to eNpHR (Lenti-CaMKIIα-eNpHR-EYFP-WPRE) was injected into the lateral ventricle of 3-d-old pups (36). Permanent denervation procedures on the right forepaw (21) were performed on 7-wk-old rats expressing eNpHR. Nondenervated rats expressing eNpHR served as controls. Three to four weeks after denervation, an optic fiber coupled to a 594-nm wavelength laser was mounted directly over the exposed craniotomy window above the right S1, and the neuronal activity of the healthy cortex (contralateral to the intact limb) was optogenetically manipulated. Multimodal in vivo

Author contributions: G.P. designed research; N.L., J.E.D., A.B.-S., A.A.G., P.W., H.K., J.J.P., N.V.T., and G.P. performed research; N.L., J.E.D., S.E.J., and G.P. analyzed data; and N.L., J.J.P., N.V.T., and G.P. wrote the paper.

The authors declare no conflict of interest.

This article is a PNAS Direct Submission.

[1]To whom correspondence should be addressed. E-mail: pelled@kennedykrieger.org.

This article contains supporting information online at www.pnas.org/lookup/suppl/doi:10.1073/pnas.1100815108/-/DCSupplemental.

techniques were applied to evaluate functional responses in the deprived S1 from the single neurons to large somatosensory network levels.

Results

A diagram of the experimental paradigm is shown in Fig. 1*A*. Immunohistochemistry was performed on brain slices obtained from all of the rats in this study (Fig. 1*B*). On average, 15% of all of the cells located within S1 that were identified with nuclear staining DAPI, which stains for both neurons and glia nuclei, were positively stained with both antienhanced YFP (EYFP; indicative of eNpHR expression) and anticalcium/calmodulin-dependent protein kinase IIα (CaMKIIα; a marker of excitatory pyramidal neurons). Because neurons consist of ~63% of all cells in the rat somatosensory cortex (37) and pyramidal neurons consist of ~80% of all neurons (38), specific expression of eNpHR was found in 29% of the pyramidal neurons population.

Single-Unit Responses. The effects of forepaw electrical stimulation and illumination of eNpHR (i.e., optical activation of eNpHR) on neuronal responses were investigated in control and denervated rats expressing eNpHR in their excitatory cortical neurons. Tungsten electrodes were slowly advanced through the right and left S1, and the extracellular firing rates of well-isolated spontaneously firing neurons were tested in response to contralateral and ipsilateral forepaw electrical stimulation and/or illumination. A total of 155 neurons from control (53 neurons, $n = 5$) and denervated (102 neurons, $n = 5$) rats were isolated. Increases in spiking responses induced by forepaw electrical stimulation (>2 SDs in the first 20 ms after stimulation onset) were determined for each of the isolated neurons (Table S1). Increases and decreases in firing rates induced by 30 s of continuous illumination of eNpHR and illumination in conjunction with forepaw electrical stimulation were tested as well. Consistent with previous reports (27), the eNpHR-mediated inhibition was found to be stable and effective over 30 s. Ten percent change in firing rate induced by 30 s of continuous illumination of eNpHR compared with 30 s of spontaneous firing rate was considered significant. Lamina-specific responses of neurons and the average change in firing rates under each condition in control and denervated rats are shown in Tables S2–S4. Because studies have shown that the transcallosal fibers form synapses on both excitatory and inhibitory neurons (39), we further aimed to determine the identity of the specific neuronal population that responded to forepaw electrical stimulation and/or increased or decreased their firing rates in response to illumination of eNpHR. One method of characterizing neurons is by the width of their action potential (AP), because it was previously shown that the durations of the second phase of the AP (i.e., refractory phase) of pyramidal neurons are longer than interneurons (20, 40–42), which are mostly inhibitory (43). Examples of firing rates of long AP duration neurons located in the deprived S1 of the denervated rat under the different conditions are illustrated in Fig. 1*C*.

In control rats, 78% of 28 isolated neurons in S1 responded to contralateral electrical stimulation. All of these neurons had long AP durations (>0.5 ms) and were located in the granular lamina IV and the infragranular laminae V and VI. Only a single neuron responded to ipsilateral forepaw electrical stimulation. Illumination of eNpHR of the right S1 by itself resulted in increases in firing rates of 17% and decreases in firing rates of 42% of neurons in the right S1 (ipsilateral to illumination and contralateral to forepaw electrical stimulation). All of these neurons exhibited long AP durations and were located in laminae IV, V, and VI. The firing rates increased in 68% and decreased in 16% of 25 neurons isolated in S1 contralateral to illumination. The majority of the neurons that increased their firing rate (69%) exhibited long AP durations and were located in laminae IV, V, and VI. Thus, in control rats, illumination of eNpHR affected the firing rates of neurons located within the light-stimulated S1 as well as the contralateral S1. Illumination of eNpHR combined with forepaw electrical stimulation did not change the tendency of the neurons to increase or decrease their firing rate compared with illumination of eNpHR alone.

In forepaw-denervated rats, 71% of 48 isolated neurons in the healthy S1 responded to contralateral intact forepaw electrical stimulation. The majority of these neurons (88%) had long AP durations and were located in laminae IV, V, and VI. Intact forepaw electrical stimulation also resulted in increases in firing rates of neurons in the deprived S1 ipsilateral to forepaw electrical stimulation (38%, 54 total neurons). Consistent with previous studies (20), the majority of these responding neurons exhibited short AP durations (<0.5 ms) and were located in the laminae V and VI (66% and 87% of responding neurons, respectively). These findings suggest that, through a neuroplasticity mechanism that involves up-regulation of inhibitory interneuron activity, input from the intact limb results in overinhibition of the deprived S1.

The firing rates of 10% and 56% of neurons located within the right healthy S1 increased and decreased, respectively, by illumination of eNpHR. The majority of these neurons (75%) exhibited long AP durations and were located in laminae IV, V, and VI. Illumination of eNpHR of the healthy S1 resulted in increases in firing rates of 61% and decreases in firing rates of

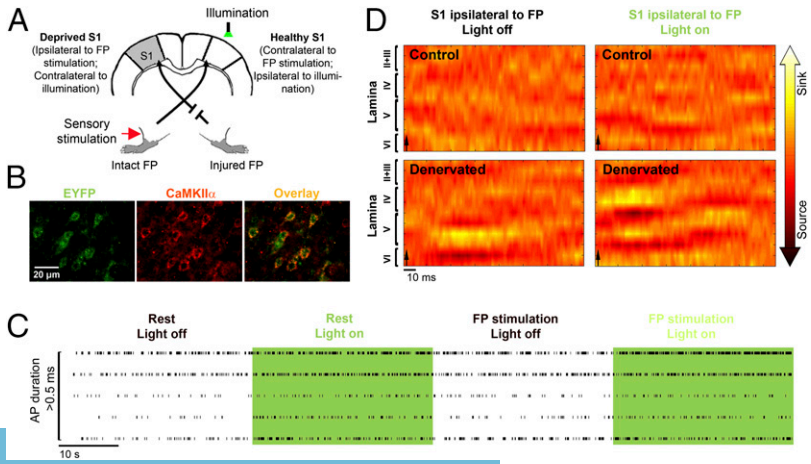

Fig. 1. Electrophysiology shows increased excitatory neuronal activity within the deprived S1 by illumination of eNpHR. (*A*) A diagram illustrating the experimental design (S1, primary somatosensory cortex; FP, forepaw). (*B*) Examples of neurons within S1 immunostained with antibodies targeted to EYFP (indicative of eNpHR expression) and CaMKIIα (marker of excitatory pyramidal neurons). (*C*) Five spike trains obtained from five individual neurons exhibiting long action potential (AP) durations (>0.5 ms) located within lamina V of the deprived S1 in denervated rats. Compared with the spontaneous firing rates (rest) and firing rates in response to intact forepaw electrical stimulation alone, illumination of eNpHR of the healthy S1 combined with intact forepaw electrical stimulation induced increases in the firing rates of long AP duration neurons (i.e., excitatory pyramidal cells). (*D*) Examples of current source density maps obtained from S1 ipsilateral to intact forepaw electrical stimulation show that illumination of eNpHR of the healthy S1 leads to increases in the inward currents (sink; i.e., excitation) in the deprived S1 of the denervated rats.

11% of neurons in the deprived S1 contralateral to illumination. However, illumination of eNpHR of the healthy S1 combined with intact forepaw electrical stimulation resulted in increases in firing rates of 31% and decreases in firing rates of 29% of neurons in the deprived S1 (contralateral to illumination and ipsilateral to intact forepaw electrical stimulation). One-half of the neuronal population that increased or decreased its firing rate exhibited long AP durations and was located in laminae III–VI. In addition, greater decreases in the percent changes in firing rates (as calculated according to the spontaneous firing rate) were observed in short AP durations compared with long AP durations neurons (Table S4). Thus, illumination of eNpHR of the healthy S1 combined with intact forepaw electrical stimulation caused (*i*) greater increases in firing rates of excitatory pyramidal neurons (long AP durations) and (*ii*) greater decreases in firing rates of inhibitory interneurons (short AP durations) within the deprived S1 compared with neuronal responses observed as a result of forepaw electrical stimulation alone.

Local Field Potential. Local field potential (LFP) responses to forepaw electrical stimulation and to illumination of eNpHR combined with forepaw electrical stimulation were acquired in equally spaced cortical depths ranging from 50 to 1,850 μm below the pia matter. Current source density (CSD) analysis of stimulus-induced LFP responses [according to Mitzdorf (44) and Mitzdorf and Singer (45)] was applied to identify the net transmembrane currents reflecting the neuronal inputs and outputs of S1. Specifically, CSD analysis distinguishes between inward (sink) and outward (source) neuronal currents that are thought to reflect excitation and inhibition, respectively. The laminar CSD pattern of S1 contralateral to forepaw electrical stimulation (alone or combined with illumination of eNpHR) was generally similar for the control and forepaw-denervated rats groups, where the onset of the inward currents initiated in lamina IV and extended to the supragranular and infragranular laminae. However, the CSD pattern of the deprived S1 ipsilateral to forepaw electrical stimulation showed increases in inward currents in lamina IV and infragranular lamina V by illumination of eNpHR. These results are consistent with the single-unit recordings that showed increased activity of excitatory neurons in laminae V and VI within the deprived S1 by illumination of eNpHR (Fig. 1*D*). Significant changes of the average CSD sink and source values are shown in Table S5 for control ($n = 5$) and denervated ($n = 5$) rats (Z test analysis with effective significance of $P < 0.05$).

Cerebral Blood Flow Responses. The electrophysiology measurements provided detailed characteristics of the behavior and identity of the neurons located in S1 of the denervated rats. However, only a small population of neurons could be sampled because of the nature of the method. Therefore, we aimed to determine if there is an increase in cerebral blood flow (CBF) responses associated with the increase in the firing rates of neurons within the deprived S1 of the denervated rats as a result of illumination of eNpHR. CBF responses were investigated in control ($n = 5$) and denervated ($n = 5$) rats expressing eNpHR by the method of laser speckle contrast imaging (LSCI), which is a minimally invasive imaging modality that offers functional information from the vasculature with high spatiotemporal resolution and does not require contrast agent delivery (46–48). The average magnitude of the CBF responses was measured from a 400 × 400-μm region of greatest interest; this region was selected around a cluster of 10 pixels that exhibited the highest changes in magnitude (Z test analysis with effective significance of $P < 0.05$). Examples of CBF responses Z map, time courses of the CBF responses from individual rats, and group analysis are shown in Fig. 2.

The magnitude of the CBF responses to ipsilateral intact forepaw electrical stimulation within the deprived S1 was significantly increased by illumination of eNpHR of the healthy S1 compared with forepaw electrical stimulation alone ($P < 0.05$). This increase in CBF in the deprived S1 concurs with the neuronal firing rates and LFP responses observed in the forepaw-denervated rats. The averaged values of the CBF responses amplitudes are shown in Table 1.

fMRI Responses. Finally, we measured if the decreases in the overinhibition of the deprived S1 in denervated rats caused by transcallosal manipulations by illumination of eNpHR were sufficiently robust to be visualized in a noninvasive manner. Blood oxygenation level-dependent (BOLD) fMRI responses were assessed in control ($n = 5$) and denervated ($n = 5$) rats expressing eNpHR in a 9.4-T horizontal animal scanner, which permitted high spatial (150 × 150 × 1,000 μm) and temporal (1,000 ms) resolution. A custom-built MRI holder was equipped with a dedicated device for positioning the optic fiber to transmit the illumination. For each condition (left forepaw electrical stimulation with and without illumination of eNpHR of the right S1), the number of activated pixels ($P < 0.05$) was calculated across three 1-mm-thick slices representing S1. Fig. 3 shows BOLD fMRI activation Z map of individual control and denervated rats overlaid on high-resolution anatomical MRI images [Bregma 1.5 mm according to Paxinos and Watson (49)] and group statistics.

The extent of the BOLD responses to ipsilateral intact forepaw electrical stimulation within the deprived S1 significantly increased by illumination of eNpHR of the healthy S1 compared with forepaw electrical stimulation alone ($P < 0.05$). These results are consistent with the findings obtained by the earlier electrophysiology recordings and CBF measurements. The averaged values of the BOLD activation extent are shown in Table 1.

Discussion

Human (2) and animal (17, 18) studies have shown that distortions of the cortical representation occur within minutes after

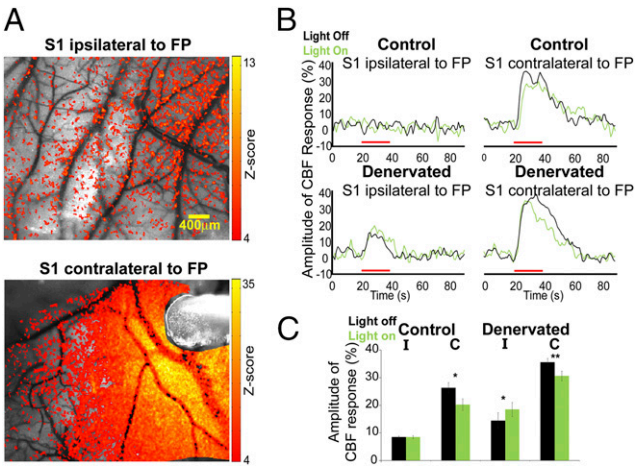

Fig. 2. Optical imaging shows increased cerebral blood flow responses within the deprived S1 by illumination of eNpHR. (*A*) Examples of LSCI CBF *z* activation maps overlaid on original CBF contrast images obtained from healthy [contralateral to forepaw (FP) electrical stimulation] and deprived (ipsilateral to FP electrical stimulation) S1 in denervated rats. Illumination of eNpHR was delivered through an optic fiber, which can be visualized in *Lower* image. (*B*) In denervated rats, illumination of eNpHR of the healthy S1 resulted in increased CBF responses in the deprived S1 ipsilateral to intact FP electrical stimulation. Red bars represent FP electrical stimulation. (*C*) Group average of the CBF responses amplitude changes in S1 contralateral (C) and ipsilateral (I) to FP electrical stimulation in control ($n = 5$) and denervated ($n = 5$) rats with or without illumination of eNpHR (*$P < 0.05$; **$P < 0.005$).

Table 1. Average values of the CBF response amplitude and BOLD activation extent

	Control		Denervated	
	S1 ipsilateral to FP	S1 contralateral to FP	S1 ipsilateral to FP	S1 contralateral to FP
CBF (percent amplitude of CBF response)				
Light off	8.48 ± 0.33	26.25 ± 1.90	14.39 ± 2.90	35.56 ± 1.35
Light on	8.45 ± 0.54	20.20 ± 2.13*	18.43 ± 2.53*	30.59 ± 1.72†
BOLD fMRI (number of activated pixels)				
Light off	13.00 ± 3.15	151.75 ± 12.00	24 ± 2.75	215.75 ± 15.75
Light on	18.40 ± 1.34	123.25 ± 10.97*	37.4 ± 2.57*	159.25 ± 13.75*

The averaged values (± SEM) are shown for control and denervated rats in primary somatosensory cortex (S1) contralateral and ipsilateral to forepaw (FP) electrical stimulation with or without illumination of eNpHR over the right healthy S1.
*$P < 0.05$.
†$P < 0.005$.

nerve injury, suggesting a neuroplasticity process that involves unmasking of previously present but functionally inactive synaptic connections. Essentially, this process changes the balance between excitation and inhibition, a change that is reflected in altered neuronal responses in the deprived cortex, which can persist for weeks and months after injury. Modifications in synaptic transmission, yielding increased excitability in sensory and motor cortical representations both contralateral and ipsilateral to the injury, are an important neuroplasticity mechanism underlying cortical reorganization. For example, the extent of the somatosensory cortex reorganization after nerve injury was reduced after systemic administration of NMDA antagonist (50, 51) and was tightly correlated to NMDA receptor-mediated plasticity (52). Increases in cortical excitability were also shown to be accompanied by increases in AMPA receptor autoradiographic binding (53) and decreases in GABA staining in the deprived S1 (53, 54). Moreover, increases in motor-evoked potential in the motor cortical representations contralateral and ipsilateral to the nerve injury in human subjects were blocked after administration of GABA agonists (24).

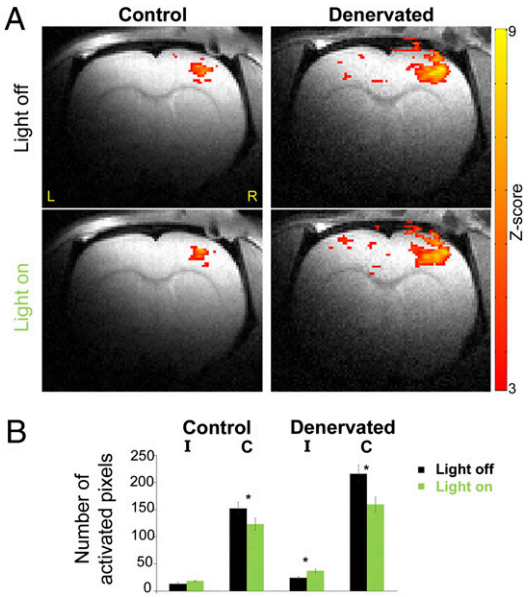

Fig. 3. fMRI shows increased BOLD responses within the deprived S1 by illumination of eNpHR. (*A*) In denervated rats, illumination of eNpHR of the healthy S1 induced increases in BOLD fMRI responses in the deprived S1 ipsilateral to intact FP stimulation. *Z* maps ($P < 0.05$) are overlaid on the anatomical images. (*B*) Group average of the BOLD fMRI response spatial extent in S1 contralateral (C) and ipsilateral (I) to forepaw electrical stimulation in control ($n = 5$) and denervated ($n = 5$) rats with or without illumination of eNpHR (*$P < 0.05$).

Other studies showed that sensory deprivation can lead to increases in inhibition of neuronal circuits through either long-term depression of excitatory intracortical synapses (55) or potentiation of inhibitory synapses (56). Additional evidence indicates that the increase of inhibitory neuronal activity in the deprived cortex may be the foundation of the poor recovery and pain observed in patients suffering from nerve injury (24, 25, 57). Moreover, previous studies suggested that these evoked increases in inhibitory activity are mediated through the transcallosal pathway (20, 21). The overinhibition of the deprived cortex may be adversely affecting recovery and repair by two pathways. First, the lack of excitatory cortical output from the deprived S1 may be delaying recruitment of subcortical pathways that could potentially aid in compensation (58). Second, changes in the cortical–cortical communication may interfere with normal neuronal processing in the healthy cortex (1). An emerging concept in rehabilitation is guided neuroplasticity, where the dynamic potential of neuroplasticity mechanisms is used clinically to strengthen or promote specific cortical functions (59). In our study, an optogenetic approach was used to induce such neuroplasticity by guiding and reshaping the transcallosal pathway activity that underlies cortical reorganization after nerve injury. The results show that optogenetic manipulation of the transcallosal pathway concurrent with electrical stimulation induced a substantial effect on neuroplasticity and cortical processing. This effect could be visualized with high-resolution electrophysiology and optical imaging by LSCI method as well as noninvasive fMRI.

We introduced the viral vectors into the cerebral lateral ventricles in the developing brain, because it has been shown to be an effective method to achieve widespread gene delivery in cortical and subcortical structures (36). The lentivirus intraventricular injections yielded successful eNpHR expression in approximately one-third of all pyramidal neuron population located within S1, which in consequence, elicited substantial affects on neuronal responses due to transcallosal modulations. Nevertheless, an improved method to introduce viral vectors that could infect a larger cell population might result in even greater affects on neuronal responses.

The results show that forepaw denervation altered the balance between excitation and inhibition in the deprived cortex and resulted in overall increases in inhibitory interneurons activity. Because it is evident that the molecular basis of cortical reorganization after peripheral nerve injury involves dynamic cross-talk of several synaptic mechanisms, it is likely that both increases in intracortical excitation and inhibition processes were involved. The loss of the excitatory thalamic input in the deprived hemisphere contralateral to the injured limb could have led to the emergence of inputs originating from the transcallosal

projections that have a minor contribution to cortical processing under normal conditions. Indeed, the single-unit and LFP responses showed that temporarily silencing the firing of excitatory pyramidal neurons located within the healthy S1 by illumination of eNpHR facilitates increases in the excitatory and decreases in the inhibitory, neuronal activities in the deprived S1. These effects were found in the supragranular and infragranular laminae, which is in agreement with the known anatomy of transcallosal projections (32, 33, 39). Because of the penetration characteristics of light into brain tissue, it is plausible that the primary affect on neuronal responses was mediated through the transcallosal projections originating in lamina III of the healthy S1. The firing rates of excitatory and inhibitory neurons located in the granular lamina were altered as well, suggesting that the modified neuronal activity in the infragranular laminae had a considerable affect on neuronal activity throughout the cortical laminae. Neurons in laminae VI of S1 also project to the ventral posterior lateral nucleus of thalamus (VPL). Therefore, it is conceivable that the modification in neuronal activity in lamina VI could have led to an increase in the deprived hemisphere VPL input that projects mainly on the excitatory pyramidal neurons located within the granular lamina. Indeed, excitatory pyramidal neurons have long-range axons, they form thousands of synapses with proximate and remote neurons, and their activity generates prominent excitations that drive cortical processing as well as subcortical output (60). In addition, pyramidal neurons are capable of affecting vascular responses by release of vasoactive substances (61, 62), an attribute consistent with our CBF measurements. Alterations in the neuronal firing rates exhibited by excitatory neurons and inhibitory interneurons in the deprived S1 led to a marked increase in excitatory cortical activity and correspondent CBF increases. Finally, the overall increases in excitatory neuronal activity were also reflected in the fMRI responses, strengthening the notion that fMRI can provide an appropriate platform to investigate the affect of optogenetic manipulations on the behavior of large neuronal networks (63).

Overall, these results elucidate the neuronal substrates and neuroplasticity mechanisms that mediate the altered functional responses observed in the bilateral cortical somatosensory representations. These findings could be directly translated into clinical applications in terms of improving rehabilitation strategies, which are based on bilateral cortical manipulations to achieve transcallosal modulations such as with CIT and TMS.

Materials and Methods

All animal procedures were conducted in accordance with the National Institutes of Health Guide for the Care and Use of Laboratory Animals and were approved by the Johns Hopkins University Animal Care and Use Committee.

Virus Preparation. Lentivirus production and transduction were performed using the method by Gradinaru et al. (30).

Stereotaxic Injection. The lentivirus (5 μL) was delivered to P3 rat pups under cryoanesthesia. A Hamilton needle (31 gauge) was lowered into the right lateral ventricle [anterior-posterior (AP) = 0.8 mm, medial-lateral (ML) = 2 mm, dorsal-ventral (DV) = 1.8 mm, relative to Bregma].

Forepaw Denervation. Seven-wk-old rats expressing eNpHR underwent excision of the right forepaw radial, median, and ulnar nerves as reported previously (21).

Craniotomies and Stimulation. Electrophysiology, optical imaging, and fMRI measurements were performed on 10- to 11-wk-old rats. The anesthetized rat's head was fixed in a stereotaxic frame (Kopf). A 0.5-mm region of the skull was thinned over the right and left S1 centered at AP = 1 mm and ML ± 3.6 mm. Respiration rate, PO_2, and heart rate were continuously monitored throughout all measurements (Starr Life Sciences Corp.). Illumination of eNpHR was performed on the right S1. A 10-ft-long optic fiber (400 μm diameter) was used to deliver continuous 594-nm laser light (Thorlabs) during electrophysiology, optical imaging, and fMRI measurements. The output light intensity was 16 $mWmm^{-2}$. Electrical stimulation of the forepaw consisted of 3 mA 300-μs pulses repeated at 3 Hz for 30 s (electrophysiology) and 20 s (optical imaging and fMRI). In agreement with previous studies (16, 64), forepaw electrical stimulation at 9 Hz elicited consistent and robust fMRI responses compared with forepaw electrical stimulation at 3 Hz.

Electrophysiology. Rats were anesthetized with urethane (1.25 g/kg i.p.), and 350-KΩ tungsten electrodes were placed above the center of the right and left somatosensory forepaw representations (according to Paxinos and Watson) (49) and lowered to the target depths by using micromanipulators (FHC). Extracellular single-unit and LFP recordings were obtained simultaneously (FHC). Starting at the cortical surface, spiking activity and LFP recordings were conducted in 150-μm increments until 1,900 μm. When a spike from a single neuron was identified, additional measurements of spiking activity and LFP were performed. Spikes and LFP were sampled at 25 KHz and 1,000 Hz, respectively, and bandpass-filtered between 300–5,000 Hz and 0.1–500 Hz, respectively. Discriminated signals were collected with a Cambridge Electronic Design (CED) interface and Spike2 data acquisition and analysis software. Spike sorting was conducted by principal component analysis. LFP waveforms were averaged with respect to the stimulation triggers. CSD maps were generated according to the methods of Mitzdorf (44) and Mitzdorf and Singer (45). The SD of the CSD values was calculated for each CSD map. Significant changes in the CSD sink and source values during forepaw electrical stimulation with or without illumination of eNpHR were determined using Z test ($P < 0.05$) with a threshold equal to 2.25 × SD.

Optical Imaging. Craniotomies of 4 × 5 mm over the right and left S1 were performed under isoflurane anesthesia. A 632-nm laser (0.5 mW; JDSU) provided coherent illumination for speckle imaging. Images were acquired using an 8-bit Basler camera (Basler Vision Technologies) with a 60-mm f/2.8 macrolens (Nikon). A D620/30-m filter (Chroma) was used to block the 594-nm wavelength from entering the camera. Images were acquired continuously at a rate of 25 frames per second (fps), with an exposure time of 5 ms. Five sets of data from 20 s of baseline activity followed by 20 s of forepaw electrical stimulation with or without additional illumination of eNpHR were recorded. Raw speckle images were coregistered, and the contrast was calculated according to the method by Li et al. (48). Activation maps were obtained using two-tailed Z tests ($P < 0.05$) with an activation threshold set to 3.5 and a cluster size of >10 pixels.

fMRI. After craniotomy procedures, a bolus of dexmedetomidine (0.05 mg/kg s.c.) was given, and anesthesia was then maintained by a continuous infusion (0.1 mg/kg) (16, 64). Images were acquired on a 9.4-T (Bruker) animal-dedicated MRI system. A custom-built 1.1-cm-diameter surface coil was used to transmit and receive MR signals. A single-shot, gradient echo, echo planar imaging sequence was used with the following parameters: effective echo time = 21 ms, repetition time = 1,000 ms, band width = 250 kHz, field of view = 1.92 × 1.92 cm, and matrix size = 128 × 128. The paradigm consisted of 10 dummy MRI scans to reach a steady state followed by two epochs of 20 baseline and 20 scans during forepaw electrical stimulation with or without illumination of eNpHR. The FMRIB Software Library (FSL) software was used for analysis (65). Activation maps were obtained using the general linear model. Z statistic results were cluster-size thresholded for effective significance of $P < 0.05$. The activation threshold was set at 2.3. The number of activated pixels ($P < 0.05$) was calculated across three regions of interest representing S1 according to the coordinates from Paxinos and Watson (49).

Statistics. A two-tailed paired Student t test was performed between the different stimulation conditions using Matlab (Mathworks). Results and figures show the average ± SEM.

Immunohistochemistry. Immunostaining of EYFP, CaMKIIα, and DAPI was performed on 50-μm free-floating brain sections according to the method by Gradinaru et al. (30). Confocal fluorescence images were acquired using a scanning laser Olympus BX61 microscope (Olympus). ImageJ software (National Institutes of Health) was used to count the cells within the right S1 granular zone (where illumination of eNpHR was performed) that were positively stained for DAPI, EYFP, and CaMKIIα. These cells were found across the cortical depth at laminae II–VI.

ACKNOWLEDGMENTS. The authors thank Dr. Karl Deisseroth for providing the eNpHR plasmids, Dr. Abdel-Monem El-Sharkawy for designing the MRI surface coil, and Dr. Peter van Zijl and Dr. Alan Koretsky for critical reading of the manuscript. This work was supported by National Institutes of Health, National Institute of Neurological Disorders and Stroke Grant 1R01NS072171-01 (to G.P.).

1. Lundborg G (2003) Richard P. Bunge memorial lecture. Nerve injury and repair—a challenge to the plastic brain. *J Peripher Nerv Syst* 8:209–226.
2. Wall JT, Xu J, Wang X (2002) Human brain plasticity: An emerging view of the multiple substrates and mechanisms that cause cortical changes and related sensory dysfunctions after injuries of sensory inputs from the body. *Brain Res Brain Res Rev* 39:181–215.
3. Merzenich MM, et al. (1983) Progression of change following median nerve section in the cortical representation of the hand in areas 3b and 1 in adult owl and squirrel monkeys. *Neuroscience* 10:639–665.
4. Rajan R, Irvine DR, Wise LZ, Heil P (1993) Effect of unilateral partial cochlear lesions in adult cats on the representation of lesioned and unlesioned cochleas in primary auditory cortex. *J Comp Neurol* 338:17–49.
5. Melzer P, Smith CB (1998) Plasticity of cerebral metabolic whisker maps in adult mice after whisker follicle removal—I. Modifications in barrel cortex coincide with reorganization of follicular innervation. *Neuroscience* 83:27–41.
6. Pluto CP, Chiaia NL, Rhoades RW, Lane RD (2005) Reducing contralateral SI activity reveals hindlimb receptive fields in the SI forelimb-stump representation of neonatally amputated rats. *J Neurophysiol* 94:1727–1732.
7. Stojic AS, Lane RD, Killackey HP, Rhoades RW (2000) Suppression of hindlimb inputs to S-I forelimb-stump representation of rats with neonatal forelimb removal: GABA receptor blockade and single-cell responses. *J Neurophysiol* 83:3377–3387.
8. Abo M, Chen Z, Lai LJ, Reese T, Bjelke B (2001) Functional recovery after brain lesion—contralateral neuromodulation: An fMRI study. *Neuroreport* 12:1543–1547.
9. Caramia MD, Iani C, Bernardi G (1996) Cerebral plasticity after stroke as revealed by ipsilateral responses to magnetic stimulation. *Neuroreport* 7:1756–1760.
10. Dijkhuizen RM, et al. (2001) Functional magnetic resonance imaging of reorganization in rat brain after stroke. *Proc Natl Acad Sci USA* 98:12766–12771.
11. Kim YH, et al. (2003) Bilateral primary sensori-motor cortex activation of post-stroke mirror movements: An fMRI study. *Neuroreport* 14:1329–1332.
12. Kim YR, et al. (2005) Measurements of BOLD/CBV ratio show altered fMRI hemodynamics during stroke recovery in rats. *J Cereb Blood Flow Metab* 25:820–829.
13. Luke LM, Allred RP, Jones TA (2004) Unilateral ischemic sensorimotor cortical damage induces contralesional synaptogenesis and enhances skilled reaching with the ipsilateral forelimb in adult male rats. *Synapse* 54:187–199.
14. Reinecke S, Dinse HR, Reinke H, Witte OW (2003) Induction of bilateral plasticity in sensory cortical maps by small unilateral cortical infarcts in rats. *Eur J Neurosci* 17: 623–627.
15. Rema V, Ebner FF (2003) Lesions of mature barrel field cortex interfere with sensory processing and plasticity in connected areas of the contralateral hemisphere. *J Neurosci* 23:10378–10387.
16. Pawela CP, et al. (2010) Interhemispheric neuroplasticity following limb deafferentation detected by resting-state functional connectivity magnetic resonance imaging (fcMRI) and functional magnetic resonance imaging (fMRI). *Neuroimage* 49:2467–2478.
17. Calford MB, Tweedale R (1990) Interhemispheric transfer of plasticity in the cerebral cortex. *Science* 249:805–807.
18. Shin HC, et al. (1997) Interhemispheric modulation of sensory transmission in the primary somatosensory cortex of rats. *Neurosci Lett* 230:137–139.
19. van Meer MP, van der Marel K, Otte WM, Berkelbach van der Sprenkel JW, Dijkhuizen RM (2010) Correspondence between altered functional and structural connectivity in the contralesional sensorimotor cortex after unilateral stroke in rats: A combined resting-state functional MRI and manganese-enhanced MRI study. *J Cereb Blood Flow Metab* 30:1707–1711.
20. Pelled G, et al. (2009) Ipsilateral cortical fMRI responses after peripheral nerve damage in rats reflect increased interneuron activity. *Proc Natl Acad Sci USA* 106: 14114–14119.
21. Pelled G, Chuang KH, Dodd SJ, Koretsky AP (2007) Functional MRI detection of bilateral cortical reorganization in the rodent brain following peripheral nerve deafferentation. *Neuroimage* 37:262–273.
22. Björkman A, Rosén B, Lundborg G (2005) Enhanced function in nerve-injured hands after contralateral deafferentation. *Neuroreport* 16:517–519.
23. Rosén B, Björkman A, Lundborg G (2006) Improved sensory relearning after nerve repair induced by selective temporary anaesthesia—a new concept in hand rehabilitation. *J Hand Surg Br* 31:126–132.
24. Werhahn KJ, Mortensen J, Kaelin-Lang A, Boroojerdi B, Cohen LG (2002) Cortical excitability changes induced by deafferentation of the contralateral hemisphere. *Brain* 125:1402–1413.
25. Karl A, Birbaumer N, Lutzenberger W, Cohen LG, Flor H (2001) Reorganization of motor and somatosensory cortex in upper extremity amputees with phantom limb pain. *J Neurosci* 21:3609–3618.
26. Han X, Boyden ES (2007) Multiple-color optical activation, silencing, and desynchronization of neural activity, with single-spike temporal resolution. *PLoS One* 2:e299.
27. Zhang F, et al. (2007) Multimodal fast optical interrogation of neural circuitry. *Nature* 446:633–639.
28. Petreanu L, Huber D, Sobczyk A, Svoboda K (2007) Channelrhodopsin-2–assisted circuit mapping of long-range callosal projections. *Nat Neurosci* 10:663–668.
29. Tønnesen J, Sørensen AT, Deisseroth K, Lundberg C, Kokaia M (2009) Optogenetic control of epileptiform activity. *Proc Natl Acad Sci USA* 106:12162–12167.
30. Gradinaru V, Mogri M, Thompson KR, Henderson JM, Deisseroth K (2009) Optical deconstruction of parkinsonian neural circuitry. *Science* 324:354–359.
31. Han X, et al. (2009) Millisecond-timescale optical control of neural dynamics in the nonhuman primate brain. *Neuron* 62:191–198.
32. Wise SP, Jones EG (1976) The organization and postnatal development of the commissural projection of the rat somatic sensory cortex. *J Comp Neurol* 168:313–343.
33. Hayama T, Ogawa H (1997) Regional differences of callosal connections in the granular zones of the primary somatosensory cortex in rats. *Brain Res Bull* 43:341–347.
34. Wise SP, Jones EG (1978) Developmental studies of thalamocortical and commissural connections in the rat somatic sensory cortex. *J Comp Neurol* 178:187–208.
35. Jones EG (1975) Lamination and differential distribution of thalamic afferents within the sensory-motor cortex of the squirrel monkey. *J Comp Neurol* 160:167–203.
36. Passini MA, Wolfe JH (2001) Widespread gene delivery and structure-specific patterns of expression in the brain after intraventricular injections of neonatal mice with an adeno-associated virus vector. *J Virol* 75:12382–12392.
37. Miller MW, Potempa G (1990) Numbers of neurons and glia in mature rat somatosensory cortex: Effects of prenatal exposure to ethanol. *J Comp Neurol* 293:92–102.
38. Lübke J, Feldmeyer D (2007) Excitatory signal flow and connectivity in a cortical column: Focus on barrel cortex. *Brain Struct Funct* 212:3–17.
39. Karayannis T, Huerta-Ocampo I, Capogna M (2007) GABAergic and pyramidal neurons of deep cortical layers directly receive and differently integrate callosal input. *Cereb Cortex* 17:1213–1226.
40. Mountcastle VB, Talbot WH, Sakata H, Hyvärinen J (1969) Cortical neuronal mechanisms in flutter-vibration studied in unanesthetized monkeys. Neuronal periodicity and frequency discrimination. *J Neurophysiol* 32:452–484.
41. Simons DJ (1978) Response properties of vibrissa units in rat SI somatosensory neocortex. *J Neurophysiol* 41:798–820.
42. Tierney PL, Dégenètais E, Thierry AM, Glowinski J, Gioanni Y (2004) Influence of the hippocampus on interneurons of the rat prefrontal cortex. *Eur J Neurosci* 20:514–524.
43. Markram H, et al. (2004) Interneurons of the neocortical inhibitory system. *Nat Rev Neurosci* 5:793–807.
44. Mitzdorf U (1985) Current source-density method and application in cat cerebral cortex: Investigation of evoked potentials and EEG phenomena. *Physiol Rev* 65:37–100.
45. Mitzdorf U, Singer W (1977) Laminar segregation of afferents to lateral geniculate nucleus of the cat: An analysis of current source density. *J Neurophysiol* 40:1227–1244.
46. Murari K, et al. (2007) Contrast-enhanced imaging of cerebral vasculature with laser speckle. *Appl Opt* 46:5340–5346.
47. Dunn AK, Bolay H, Moskowitz MA, Boas DA (2001) Dynamic imaging of cerebral blood flow using laser speckle. *J Cereb Blood Flow Metab* 21:195–201.
48. Li N, et al. (2009) High spatiotemporal resolution imaging of the neurovascular response to electrical stimulation of rat peripheral trigeminal nerve as revealed by in vivo temporal laser speckle contrast. *J Neurosci Methods* 176:230–236.
49. Paxinos G, Watson C (1986) *The Rat Brain in Stereotaxic Coordinates* (Academic, Orlando, FL), 2nd Ed.
50. Garraghty PE, Muja N (1996) NMDA receptors and plasticity in adult primate somatosensory cortex. *J Comp Neurol* 367:319–326.
51. Myers WA, Churchill JD, Muja N, Garraghty PE (2000) Role of NMDA receptors in adult primate cortical somatosensory plasticity. *J Comp Neurol* 418:373–382.
52. Mowery TM, Garraghty PE (2009) Nerve-injury induced changes to GluR1 and GluR2/3 sub-unit expression in area 3b of adult squirrel monkeys: Developmental recapitulation? *Front Syst Neurosci* 3:1–7.
53. Garraghty PE, Arnold LL, Wellman CL, Mowery TM (2006) Receptor autoradiographic correlates of deafferentation-induced reorganization in adult primate somatosensory cortex. *J Comp Neurol* 497:636–645.
54. Garraghty PE, LaChica EA, Kaas JH (1991) Injury-induced reorganization of somatosensory cortex is accompanied by reductions in GABA staining. *Somatosens Mot Res* 8:347–354.
55. Rittenhouse CD, Shouval HZ, Paradiso MA, Bear MF (1999) Monocular deprivation induces homosynaptic long-term depression in visual cortex. *Nature* 397:347–350.
56. Maffei A, Nataraj K, Nelson SB, Turrigiano GG (2006) Potentiation of cortical inhibition by visual deprivation. *Nature* 443:81–84.
57. Dettmers C, et al. (2001) Increased excitability in the primary motor cortex and supplementary motor area in patients with phantom limb pain after upper limb amputation. *Neurosci Lett* 307:109–112.
58. Cauraugh JH, Summers JJ (2005) Neural plasticity and bilateral movements: A rehabilitation approach for chronic stroke. *Prog Neurobiol* 75:309–320.
59. Duffau H (2006) Brain plasticity: From pathophysiological mechanisms to therapeutic applications. *J Clin Neurosci* 13:885–897.
60. DeFelipe J, Fariñas I (1992) The pyramidal neuron of the cerebral cortex: Morphological and chemical characteristics of the synaptic inputs. *Prog Neurobiol* 39:563–607.
61. Cauli B, Hamel E (2010) Revisiting the role of neurons in neurovascular coupling. *Front Neuroenergetics* 2:1–8.
62. Drake CT, Iadecola C (2007) The role of neuronal signaling in controlling cerebral blood flow. *Brain Lang* 102:141–152.
63. Lee JH, et al. (2010) Global and local fMRI signals driven by neurons defined optogenetically by type and wiring. *Nature* 465:788–792.
64. Zhao F, Zhao T, Zhou L, Wu Q, Hu X (2008) BOLD study of stimulation-induced neural activity and resting-state connectivity in medetomidine-sedated rat. *Neuroimage* 39: 248–260.
65. Smith SM, et al. (2004) Advances in functional and structural MR image analysis and implementation as FSL. *Neuroimage* 23 (Suppl 1):S208–S219.